New Insights into Aristarchus Crater with LRO LAMP Far-Ultraviolet Observations

Elizabeth Czajka[1,2], Kurt Retherford[2,1], Georgiana Kramer[3], Amanda Hendrix[3], Joshua Cahill[4], Benjamin Byron[5], Benjamin Greenhagen[4], Thomas Greathouse[2], Lizeth Magaña[4], Kathleen Mandt[4,6], Cesare Grava[2]

Abstract

Aristarchus crater is a Copernican-age impact crater well-known for its high albedo ejecta blanket and nearby flow features rich in pyroclastic materials. The Lyman Alpha Mapping Project (LAMP) is a far-ultraviolet (far-UV) spectrograph (57-197 nm) onboard the Lunar Reconnaissance Orbiter. LAMP data identified Aristarchus crater as having **a** high Off-band (155-184 nm) to On-band (130-155 nm) albedo (Off/On) ratio, providing new insight to the mineral composition of the area. Previous LAMP observations of bright crater rays and lunar swirls show that regions of high Off/On band ratios may indicate highly feldspathic compositions. In this study we use LAMP data to understand far-UV compositional signatures at Aristarchus. We investigate **four** well characterized regions of interest around Aristarchus crater, and we compare Off/On band ratios at Aristarchus crater to laboratory-derived ratios of several endmembers such as anorthite and olivine. We further analyze LAMP far-UV spectra alongside near-infrared (near-IR) spectra from the Moon Mineral Mapper (M^3) onboard Chandrayaan-1 to characterize the mineralogy in several regions of interest. We find that LAMP Off/On band ratios are able to distinguish between plagioclase feldspars and minerals such as quartz and mafic dominated compositions. The LAMP Off/On band ratios at Aristarchus are higher than previously reported ratios for plagioclase rich regions, suggesting the composition is unique to Aristarchus. Spectra from LAMP and M^3 both show the central peak and high albedo ejecta around Aristarchus contains shocked, possibly alkalic, plagioclase feldspar.

---

[1] Department of Physics and Astronomy, University of Texas at San Antonio, 1 UTSA circle, San Antonio TX 78249, USA; Elizabeth.Czajka@contractor.swri.org

[2] Space Science and Engineering Department, Southwest Research Institute, 6220 Culebra Rd., San Antonio TX 78238, USA

[3] Planetary Science Institute, 1700 East Fort Lowell, Suite 106, Tucson, AZ 85719, USA

[4] Johns Hopkins University, Applied Physics Laboratory, 11100 Johns Hopkins Rd., Laurel, MD 20723, USA

[5] Jet Propulsion Laboratory, California Institute of Technology, 4800 Oak Grove Dr., Pasadena, CA 91109, USA

[6] NASA Goddard Space Flight Center, 8800 Greenbelt Rd, Greenbelt, MD, USA.

1. Introduction

1.1. Aristarchus

Aristarchus is a high albedo Copernican age impact crater surrounded by flow features rich in pyroclastic materials **similar to** Vallis Scheröteri (Zisk et al. 1977; Glotch et al. 2021). The origin and composition of Aristarchus' ejecta blanket has been studied since the 1960's and is a high priority science target for current and previous lunar missions, including the Lunar Reconnaissance Orbiter (LRO) (McEwen et al. 1994; Chevrel et al. 2009; Glotch et al. 2010; Glotch et al. 2021). The Aristarchus plateau is detectable and observed in LRO Lyman Alpha Mapping Project (LAMP) global maps as an area of low Lyman-alpha albedo (Cahill et al. 2019), and high Off band (155.57-189.57 nm)/On band (129.57-155.57 nm) albedo ratio (Figure 1), and positive Off-band spectral slope (Figure 1; Byron et al. 2020). **In previous studies far-ultraviolet spectral bands were chosen to investigate water ice abundance at the lunar poles (Gladstone et al. 2012). The On band (129.57-155.57 nm) and Off band (155.57-189.57 nm) were chosen due to water ice having low and high reflectance, respectively, at those two wavelength bands. LAMP Off/On band maps were then used to identify water ice exposures at the lunar poles (Gladstone et al. 2012; Magaña et al. 2022), and subsequent studies found the maps were also useful for investigating mare and highland regolith composition (Hendrix et al. 2016; Byron et al. 2021).**

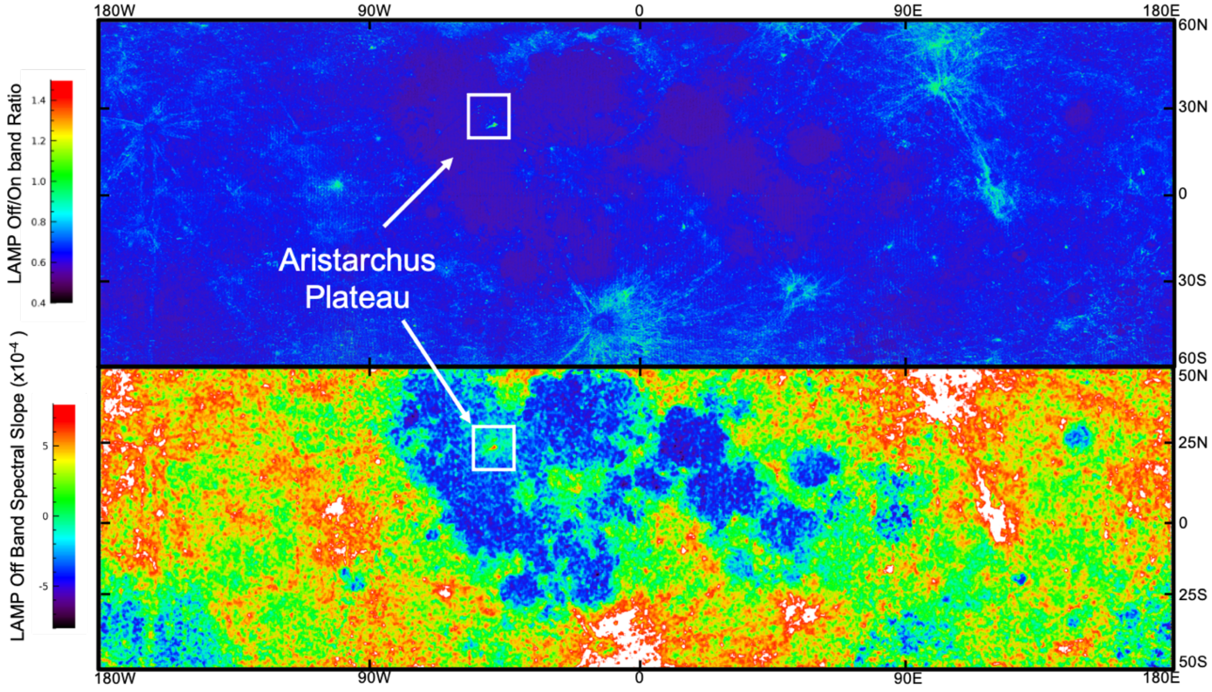

Figure 1: (Top) LAMP global maps Off/On band albedo ratio map **with ~32 pixel/degree resolution, covering -180 to 180 longitude, and -60 to 60 latitude**; (Bottom) Off band (155.57-189.57 nm) spectral slope map **with ~32 pixel/degree resolution, covering -180 to 180 longitude, and -50 to 50 latitude (**Byron et al. 2021). Aristarchus crater and the surrounding plateau stand out from the maria with elevated values in both the Off/On band ratio map and Off band spectral slope map.

It is widely thought that basaltic mare volcanism, which created the pyroclastic deposit at Aristarchus plateau, ceased around 3.0-3.8 Ga (Braden et al. 2014; Hurwitz et al. 2013). Multiple studies argue the Aristarchus impact excavated pyroclastic material created by early lunar volcanic activity along with feldspathic mantling material (Chevrel et al. 2009; Zisk et al. 1977). Other studies point to a nearby irregular mare patch and a series of sinuous rilles that originate at Aristarchus crater as evidence of lunar volcanism as recently as 1.0 to 1.5 Ga (Braden et al. 2014; Hurwitz et al. 2013).

Volcanic features produced by non-mare volcanism are often characterized by the presence of KREEP, a volcanic lithology rich in potassium (K), rare earth elements (REE) and phosphorus (P) as well as nearby thorium anomalies that produce heat and allow for a slower cooling of the silicate/alkaline magma (Jolliff et al. 2011; Braden et al. 2009; Braden et al. 2014; Hagerty et al. 2009). The irregular mare patch, and previously characterized thorium deposit, combined with low titanium measured by Clementine, make a strong case for recent non-mare lunar volcanism at Aristarchus crater (Hagerty et al. 2009; Braden et al. 2014; Zhang et al. 2014). However, compositional and petrological evidence confirming the presence of KREEP or alkaline-rich silicic minerals at Aristarchus has not been conclusively identified, leading to disagreements about the volcanic history of Aristarchus plateau, the presence of silicic lava flows and feldspathic deep mantle material (Chevrel et al. 2009; Mustard et al. 2011; Braden et al. 2014).

Mineral deposits of anorthite [$CaAl_2Si_2O_8$] (central peak), olivine [[Mg,Fe]SiO_2] (**Ea**st of crater rim), impact-melt glass (Northeast of crater rim**), and a less characterized high albedo deposit (Southwest of crater rim)** at Aristarchus have been identified and independently confirmed through analysis of Clementine, Chandrayaan-1's Moon Mineral Mapper (M^3), and LRO's Diviner Lunar Radiometer Experiment (Figure 2; McEwen et al. 1994; Chevrel et al. 2009; Mustard et al. 2011; Arnold et al. 2016). Aristarchus crater presents a unique opportunity to study mineral deposits with fewer differences in space weathering, since these unique lithologies were created and/or exposed during the same impact event (Zisk et al. 1977; McEwen et al. 1994; Chevrel et al. 2009). These relatively immature mineral deposits make Aristarchus a good case study for analyzing compositional signatures of feldspars, mafic minerals and impact melts in multi-wavelength albedo observations. We use observations from the LRO-LAMP far-UV instrument, combined with near-IR observations from the M^3 onboard the Chandryaan-1 spacecraft, to analyze the composition of the Aristarchus high albedo ejecta blanket and surrounding areas, and shed more light on the volcanic history at Aristarchus.

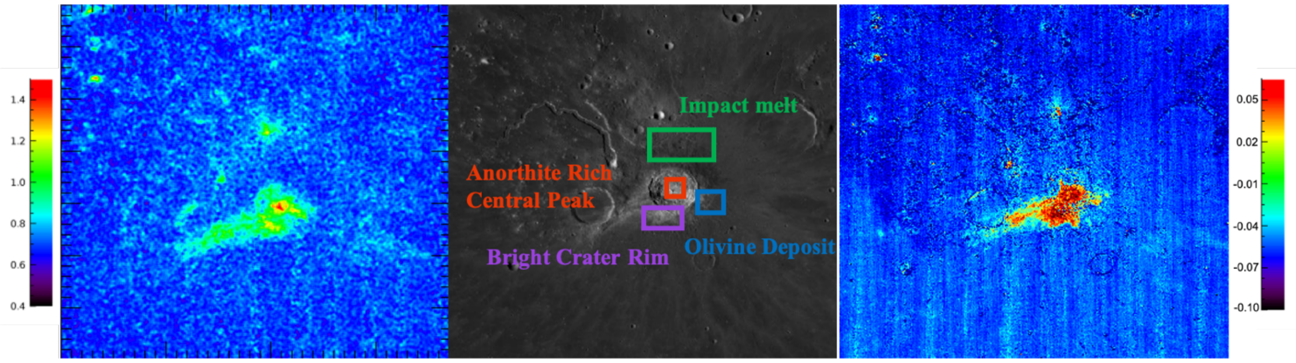

Figure 2: Aristarchus Maps; (Left) LAMP ratio of Off (155-184 nm) over On (130-155 nm) band ratio, (Center) LROC WAC monochrome mosaic (Adapted from LROC Quickmap), (Right) Diviner concavity index map (scaled -0.10 to 0.05; blue to red). Mineral deposits (center) were previously identified utilizing Clementine (McEwen et al. 1994; Chevrel et al. 2009), M^3 (Mustard et al. 2011), and Diviner (Arnold et al. 2015).

2. Observations and Methods

2.1. LAMP Observations

The LRO-LAMP instrument is a far-UV spectrograph (57-197 nm) with a 0.3° x 6.0° field-of-view (FOV) that operates in push-broom format and passively collects light reflected from the lunar surface. Incoming light is focused with an off-axis paraboloidal mirror into the entrance slit and imaged onto a holographic diffraction grating, where the light is dispersed onto a 1024 x 32-pixel microchannel plate detector (Gladstone et al. 2010). LAMP has two operating modes, enabling observations of the Moon during both sunlit (daytime) and UV starlit (nighttime) time periods. For dayside observations, LAMP used an aperture door with a small pinhole to observe the sunlit lunar surface. For nightside observations the aperture door opens, allowing a greater throughput of light to the detector for LAMP to observe UV starlight reflected off the lunar surface. A detailed explanation of the dayside and nightside LAMP albedo calculation and correction procedures can be found in Liu et al. 2018.

We limit our analysis to LAMP dayside observations of Aristarchus crater taken from October 2009 to October 2016. In October of 2016 LAMP permanently opened its fail-safe door, increasing the amount of light allowed through the slit. This new operating mode allows LAMP to obtain better signal to noise ratios for both daytime and nighttime observation modes, and requires additional calibration studies. Consequently, we limit our observations to those taken **during the seven-year period** before the failsafe door was opened. The daytime LAMP albedo maps used in this study were created with the LAMP "Global Mapper" pipeline to combine LAMP observations of the lunar surface into Off band (155.57-189.57 nm) and On band (129.57-155.57 nm) **global equatorial** maps **(with a resolution of** 32 pixels per degre**e)**, which are ratioed to create the Off/On band ratio maps (Figure **1 and** 2; **Gladstone et al. 2012)**. Daytime LAMP albedo spectra were created using the LAMP "Spectral Mapper" tool, which **combines** LAMP observations **over a region of interest** into a far-UV 3-D spectral image cube. **The spectral data cubes produced in the Spectral Mapper data pipeline use SNR weighted sum algorithms to improve data quality. A more detailed explanation of the methods and algorithms involved is currently in preparation for publication.**

The Spectral Mapper data pipeline incorporates a photometric correction to remove any phase angle effects from the reflectance spectra (Liu et al. 2018). The reflectance product reported by the Spectral Mapper is a radiance factor (I/F) that has been photometrically corrected and normalized to the standard geometric angles (i=g=30°, e=0°). For consistency, we refer to this normalized I/F product from the Spectral Mapper as "albedo" throughout the paper. Although the Global Mapper Off band and On band albedo maps used to create the Off/On ratio map shown in this work did not contain the Liu et al. (2018) phase correction, we have found that any existing phase angle effects were divided out when the maps were ratioed. More detailed explanations for the Global Mapper, Spectral Mapper, and spectral data analysis methods are in preparation for publication.

2.2. Analysis of LAMP Off/On band ratios

Using the Off/On band ratio maps generated by the LAMP Global Mapper, and the M^3 maps as a reference, mineral deposits were identified in 15x15 pixel regions of interest (ROI; Figure 3). An outlier resistant mean algorithm was utilized to calculate the average Off/On band ratio for each region of interest, under the assumption that each 15x15 pixel **(14 km x 14 km)** ROI represents a relatively homogenous composition sample of each deposit. This value represents a weighted average (outlier resistant) Off band/On band albedo ratio. We then compare these average Off/On band ratio values to laboratory Off/On band values of specific compositions (Table 1). Using LAMP Off/On band ratios and spectra of the Aristarchus' central peak, olivine deposit, and impact-melt glass, we compare spectral signatures of each region in the far-UV.

2.3. Utility of Far-Ultraviolet Measurements

Laboratory reflectance studies of Apollo soil samples, terrestrial analogs, and silicates indicate far-UV spectra are sensitive to higher energy orbital transitions within minerals (Hapke et al. 1978; Wagner et al. 1987; Philipp 1966). More recent observations from LRO LAMP seem to confirm that LAMP Off (155.57-189.57 nm)/On (129.57-155.57 nm) band ratio and Off (155.57-189.57 nm) band spectral slope map products show sensitivity to feldspathic compositions and immature crater rays (Figure 1; Hendrix et al. 2016; Cahill et al. 2019; Byron et al. 2020). Understanding the far-UV sensitivity and spectral signature of feldspar endmembers, such as anorthite, will enable LAMP to map the distribution of anorthite and/or other plagioclase endmembers in the Aristarchus ejecta blanket, further constraining its composition and origin. We compare LAMP Off/On band ratios to laboratory reference spectra and lunar infrared observations to map the distribution of plagioclase endmembers in the Aristarchus ejecta blanket.

2.4. Moon Mineral Mapper (M^3**)** Observations

M^3 was a near infrared (near-IR) imaging spectrometer that was contributed by NASA to ISRO's Chandrayaan-1 mission (Pieters et al. 2009). M^3 was able to produce near-IR 3-D spectral image cubes of the lunar surface (Pieters et al. 2009). This study uses data strips from observation period 1C (OP1C) which were then mosaiced together**, using tools and corrections provided by the M^3 team**, to provide sufficient coverage of Aristarchus crater and the surrounding regions of **interest (Besse et al. 2013, Green et al. 2011)**.

2.5. Diviner Lunar Radiometer Observations

The LRO Diviner Lunar Radiometer (Diviner) instrument is a pushbroom mapping, imaging filter radiometer that measures reflected sunlight and emitted lunar thermal emission in nine spectral channels. Diviner measure the lunar surface nearly continuously, collecting highly accurate radiance for surfaces day and night across the entire lunar temperature range. Three of Diviner's spectral channels are located near 8-microns and are used to estimate the position and shape of the mid-infrared emissivity maximum, known as the Christiansen feature (CF). The CF exhibits a near parabolic shape for lunar regolith, which **is** dominated by silicate compositions and systematically shifts in positions as a function of silicate polymerization. Mafic minerals exhibit shallower CFs at longer wavelengths, **while** highly silicic minerals exhibiting deeper CFs at shorter wavelengths. Diviner was designed to characterize the CF for the most common lunar silicate compositions (anorthite, pyroxenes, and olivine) and the CF moves out of Diviner's wavelength region for highly silicic minerals (shortward) and oxides (longward). However, the shape of the CF is still diagnostic of the presence of these minerals and Glotch et al. 2010 developed the concavity index to identify them. The concavity index (Figure 2) is neutral or positive for highly silicic and oxide rich compositions and negative for typical highland and mare compositions.

For this effort, we produced a concavity index map of Aristarchus (32 pixels per degree) using data collected between 2009 and 2019 (Figure 2). We confirmed the findings first reported by Glotch et al. 2010 that the SW crater interior, rim, and eject exhibit a strong positive concavity index, which is consistent with an abundance of minerals that are more silicic than anorthite, including alkali feldspars and quartz.

3. Analysis of Regional Mineral Deposits

Our analysis is focused on four well-studied mineral deposits around Aristarchus crater (Figure 2,3). By focusing on these areas with little inferred difference in maturity, we aim to better understand LAMP's sensitivity to mineralogy in the far-UV and the composition of Aristarchus' high albedo ejecta blanket. Building on results from the central crater peak, olivine deposit and impact melt, as outlined below, we analyze Aristarchus crater's high-albedo ejecta blanket to better constrain the composition and original lithology of the area. We identify laboratory analogs for three common mineral endmembers and compare their Off/On band ratios to the LAMP observed Off/On band ratios at the following regions of interest.

3.1. Aristarchus Central Peak

The central peak of Aristarchus crater is rich in anorthositic material, and has been the topic of many studies (Figures 2,3) (McEwen et al. 1994; Chevrel et al. 2009; Glotch et al. 2021). More than one study has argued that the deposit in Aristarchus' crater center could be the calcium and iron rich plagioclase, ferroan anorthosite ($[Fe]CaAl_2Si_2O_8$) (McEwen et al. 1994; Chevrel et al. 2009). Ferroan anorthosite is thought to be a petrologic component of the lunar crust, but is not normally found within the lunar mare of Oceanus Procellarum (McEwen et al. 1994; Chevrel et al. 2009). These studies posited, amongst other hypotheses, that the anorthosite present in Aristarchus' central peak may not be crustal material, but rather evidence of an intrusive pluton. Later studies confirmed the presence of anorthite ($CaAl_2Si_2O_8$), a major component of the lunar highlands, at Aristarchus crater but were not able to specify if it was in the form of ferroan or alkali anorthosite (Arnold et al. 2016). Previous far-UV laboratory studies show that the 98-70% anorthite Apollo sample 60025.373 has a high albedo and strong red spectral slope longward of 165 nm (Wagner et al. 1987; Hapke et al. 1978; Dixen et al. 1972; James et al. 1991). We compare the laboratory Off/On band ratio of Apollo sample 60025.373 to LAMP measured Off/On band values at the Aristarchus crater central peak, to determine the sensitivity of far-UV measurements to plagioclase rich compositions.

3.2. **Olivine Deposit (East Crater Rim)**

Along the East rim of Aristarchus is an olivine ($[Mg,Fe]SiO_2$) deposit, which has been the subject of several satellite observations and subsequent studies (Figures 2,3; McEwen et al. 1994; Chevrel et al. 2009; Mustard et al. 2011; Arnold et al. 2016). Early studies concluded that pure olivine was present, although it may be mixed with impact-melt glass and/or plagioclase (McEwen et al. 1994; Chevrel et al. 2009). This is an important distinction since the olivine deposit along the crater rim of Aristarchus could be a record of the region's original regional surface lithology. In fact, Arnold et al. 2016 pointed out that mafic material containing over 90 wt.% olivine, a dunite, could indicate a deposit that is overturned mantle material, while mixtures of plagioclase and mafic materials with 40-90 wt.% olivine may point to an intrusive magnesium suite (Mg-suite) pluton as the magmatic source of the material. Using **a new** olivine index developed **specifically for** Diviner Christiansen Feature (CF) data from LRO-Diviner, Arnold et al. 2016 estimated the Aristarchus East crater rim olivine concentration to range between 54-73 wt.%, which would agree with the conclusions of earlier studies, that the unique mineral deposits at Aristarchus are the result of the exposure of an intrusive pluton (McEwen et al. 1994; Chevrel et al. 2009; Arnold et al. 2016).

Using M^3 observations of the olivine deposit, a separate study concluded that the presence of olivine with small impact-melt glass or plagioclase inclusions alone was not strong enough evidence to prove the olivine was excavated from a shallow pluton, pointing to a notable absence of olivine-rich rock elsewhere in the crater and ejecta (Mustard et al. 2011). We demonstrate below how far-UV spectroscopy is able to differentiate between olivine and plagioclase, and aid in determining what if any plagioclase is present within the Aristarchus southwest rim olivine deposit.

3.3. **Impact Melt (Northeast Crater Rim)**

The Northeast crater rim of Aristarchus is a well-studied area with impact melt from the original impact event (Figures 2,3). Impact melt compositions around Aristarchus crater are diverse (Neish et al. 2021), and there are several possible explanations for the unique variety of impact melts observed in this region. Neish et al. 2021 suggest the most probable explanation is lithic clasts outside the walls of the crater contaminating impact melts. Using near-IR data from M^3, Neish et al. 2021 were able to conduct a spectral unmixing analysis of the area, and identify endmembers in and around Aristarchus crater. They found the northeast crater rim to be rich in pyroxene materials, that also could have some mafic components mixed in (Neish et al. 2021). This location is an ideal test case for determining LAMP’s sensitivity to pyroxene and mafic mixtures.

3.4. **High Albedo ejecta (Southwest Crater Rim)**

Previous analysis of the Aristarchus’ ejecta blanket using Clementine and M^3 suggest the composition is dominated by plagioclase, with a small mafic component (Chevrel et al. 2009; Mustard et al. 2011). The excavated plagioclase could be a mixture of older buried pyroclastics and crustal material (Mustard et al. 2011; Chevrel et al. 2009; McEwen et al. 1994). Alternatively, the pyroclastics in ejecta blanket could have been produced by non-mare volcanism as late as 1.0-1.5 GA (Hagerty et al. 2009; Braden et al.

2014; Zhang et al. 2014). Aristarchus crater sits right on top of a large thorium anomaly, and the exposed pyroclastics closest to Aristarchus have thorium concentrations of ~10 ppm. Thorium concentrations that high could be consistent with the incorporation of KREEP material into the parent magma (Hagerty et al. 2009). We concentrate on a portion of the high albedo ejecta blanket along the Southwest rim of Aristarchus crater (Figures 2,3). The LAMP Off/On band ratio images are demonstrated here to effectively map the distribution of plagioclase in the ejecta blanket, which we then compare with M^3 spectra of the region to determine if KREEP or non-mare basalts could be present.

4. Results

4.1. LAMP Off/On Albedo Ratios for Region of Interest

Our analyses show that LAMP measured Off/On band albedo ratios of the Aristarchus central peak are consistent with laboratory measured Off/On band ratios for lunar anorthite ([$CaAl_2Si_2O_8$]; Table 1). This confirms previous LAMP results that attributed LAMP's high Off/On band ratio values to plagioclase feldspar-rich compositions (Hendrix et al. 2016; Byron et al. 2020).

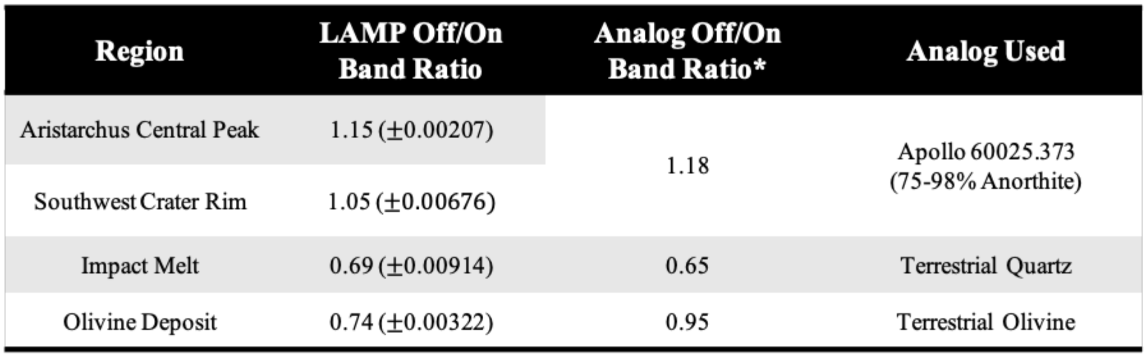

Region	LAMP Off/On Band Ratio	Analog Off/On Band Ratio*	Analog Used
Aristarchus Central Peak	1.15 (±0.00207)	1.18	Apollo 60025.373 (75-98% Anorthite)
Southwest Crater Rim	1.05 (±0.00676)		
Impact Melt	0.69 (±0.00914)	0.65	Terrestrial Quartz
Olivine Deposit	0.74 (±0.00322)	0.95	Terrestrial Olivine

Table 1: LAMP Off/On band ratio values for each region compared to laboratory analogs. *Lab spectra from Hapke et al. 1978 and Phillips et al. 1966

Lunar anorthite [$CaAl_2Si_2O_8$], has been shown to have a red slope between 160-190 nm of the far-UV (Hapke et al. 1978; Wagner et al. 1987). We observe a similar red slope in LAMP far-UV spectra of the central crater peak of Aristarchus (Figures 1 and 3). Additionally, the LAMP Off/On band albedo ratios for the impact-melt and olivine deposit are 0.69 and 0.74, respectively (Table 1). While statistically significant, a difference of 0.05 between the impact-melt and olivine LAMP Off/On band albedo ratios alone is insufficient to reliably identify differences in composition between the two mafic deposits. This is qualitatively supported by the similarity in LAMP far-UV spectra for each region (Figure 3), where both the olivine and impact-melt deposits are comparably dark at longer wavelengths and maintain a blue slope between 140-190 nm. There is also very little difference in the LAMP far-UV albedo spectra for both the crater central peak and southwest crater rim regions (Figure 3), suggesting that LAMP far-UV data alone is insufficient to determine the compositional differences between these two regions.

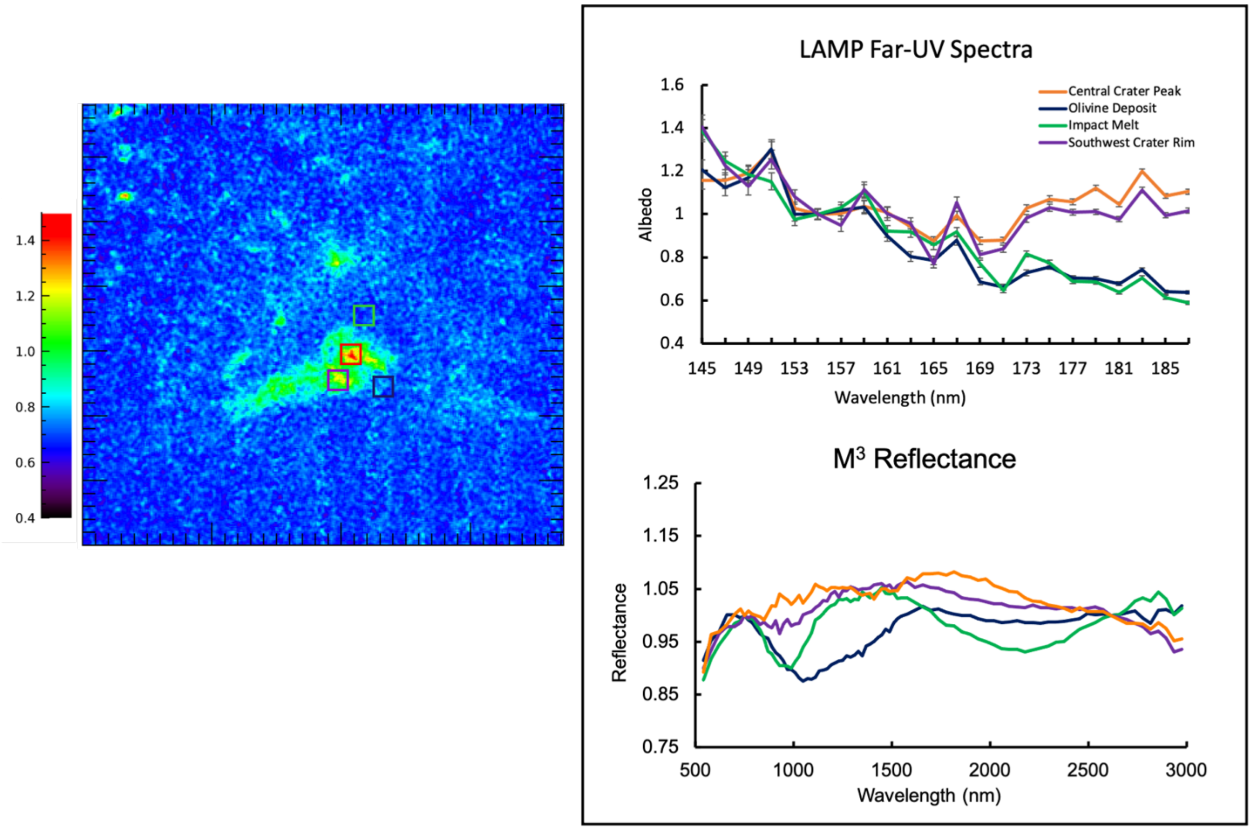

Figure 3: (Left) LAMP Off/On band albedo ratio map of Aristarchus. (Top Right) LAMP far-UV normalized albedo for regions of interest (Bottom Right) **Moon Mineral Mapper (M^3) near-infrared spectra shown with the continuum removed using two straight lines chosen at 750 and 2620 nm.** All spectra are color coded to highlighted regions in the left map.

These two pairs of regions are however distinctly different, with the crater central peak and southwest rim regions showing a reddened spectral slope longward of 170 nm relative to the impact melt and olivine deposit regions. We next describe how the near-infrared spectra collected by M^3 is critical to further characterizing the composition of this region.

4.2. M^3 Spectral Regions of Interest

Each region of interest was studied with infrared spectra from M^3. **The M^3 spectrum of Aristarchus' central peak is bright and relatively featureless with a small absorption band around 1100-1200 nm which is most consistent with a plagioclase feldspar as shown in Karr 1973 and Donaldson Hanna et al. 2014. Several factors will cause the shallow 1200 nm band that's associated with crystalline plagioclase to shift to higher or lower wavelengths and surface/shock processes cause the band to become more shallow (Karr 1975; Donaldson-Hanna et al.2014). Consequently this feature can be difficult to observe on the lunar surface and can occur anywhere from 1100-1300 nm (Karr 1975; Donaldson-Hanna et al.2014). The shallow plagioclase feature seen between 1100-1200 nm would be consisted with a low FeO content, shocked plagioclase feldspar, as was reported in Mustard et al. 2011.** The M^3 spectra also confirm the presence of an olivine deposit to the southeast of the crater rim. The 1000 nm band **typically associated with the** in the olivine deposit spectrum is broad and asymmetric (Figure 3), indicative of an iron rich olivine with less than 50 percent forsterite (Fo_{50}; Sunshine and Pieters 1998). The impact melt deposit to the north of the crater shows spectral **minima** at approximately 950 nm and 2150 nm, suggesting the impact melt is a clino-pyroxene, as shown in previous studies (Klima et al. 2007, 2011). We confirm results from Neish et al. 2021, which carried out a more detailed spectral unmixing analysis with M^3 data, and mapped pyroxene to the north of Aristarchus crater. The spectra on the southwest crater rim looks very similar to the plagioclase feldspar in the central crater peak. The southwest crater rim spectrum is bright and also shows a small absorption around 1000 nm. **This broad absorption band and relatively bright spectra is most consistent with the presence a small amount of olivine or pyroxene, indicating this is a plagioclase feldspar with a small mafic component.** This interpretation is consistent with results from Neish et al. 2021, whose M^3 spectral unmixing studies of the area concluded that the material around the southwest crater rim is more evolved and likely excavated material from the initial impact event.

5. Discussion

5.1. Mineral Deposits in Aristarchus

Based on the results shown in Table 1, LAMP Off/On band ratio values are able to distinguish between plagioclase feldspar and minerals that are dark in the far-UV such as olivine and quartz. The mineral deposits around Aristarchus crater with LAMP spectra (Figure 3) show nearly identical spectra shortward of ~170 nm. Longward of 170 nm, the LAMP spectra diverge into two distinct groups with either 1) low (0.6-0.7) or 2) high (1-1.2) normalized hemispherical albedo.

The first group, with a low (0.6-0.7) hemispherical albedo longward of 170 nm includes the olivine and impact-melt deposits. Both have relatively low Off/On band ratio values (Table 1), which is consistent with both laboratory Off/On band ratios and the full set of LAMP far-UV spectra (Figure 3). M^3 near-IR spectra of the impact-melt and olivine deposits both have distinct mafic absorption bands but no immediately discernable plagioclase feldspar absorptions near 1200 nm. Mafic-bearing mineral assemblages, including olivine and impact-melts with glassy silicates, are relatively dark and have a blue slope in the far-UV (Byron et al. 2021; Hendrix et al. 2016). The small difference in ratios for these two regions is statistically significant (Table 1) and it has been shown that with additional processing, these subtle differences can lead to more mineralogical information (Byron et al. 2021). A possible explanation for the far-UV blue slope we see in mafic-bearing minerals is that the minimum associated with the volume scattering-to-surface scattering transition is shifted to longer wavelengths (Byron et al. 2021); we discuss an alternate explanation below.

Secondly, the group with high (1.0-1.2) hemispherical albedo longward of 170 nm includes the crater’s central peak and the southwest crater rim sites. Based on LAMP Off/On band ratios in Table 1, Aristarchus crater’s central peak is consistent with an anorthositic plagioclase feldspar similar to Apollo sample 60025.373. It is worth nothing that the 15x15 pixel ROI’s were selected to ensure appropriate sampling statistics, but these could contain data from the surrounding area averaged in. This means the Off/On band values reported here may be under-estimated. Near-IR spectra from M^3 (Figure 3) confirms the crater central peak is consistent with plagioclase feldspar, and does not show evidence of pyroxene. Similarly, M^3 spectra for the southwest crater rim shows plagioclase is present, but also shows a small mafic component. Given that both sites have very little difference in the LAMP spectra, this suggests the LAMP far-UV spectra is sensitive to an electronic transition occurring around 170-190 nm in plagioclase feldspar, and may not be sensitive to mafic components mixed into the surface material. This result is consistent with other LAMP studies, which showed feldspathic-rich highlands had higher Off/On band ratios, as well as high Off band spectral slopes compared to the neighboring maria (Byron et al. 2021; Byron et al. 2020; Hendrix et al. 2016). LAMP’s Off/On band ratio maps and far-UV spectra of the crater central peak and southwest crater rim regions are consistent with a plagioclase felspar-rich composition, and is corroborated by M^3 spectra.

5.2. Far-UV Mineral Spectroscopy

Combining spectral information from multiple wavelength ranges allows us to synthesize information about both the electronic and vibrational structure of a mineral, rock or regolith. As we move to shorter wavelengths in the electromagnetic spectrum, ultraviolet absorption bands are mainly affected by quantum mechanics' derived selection rules, the symmetry of the E-field the material experiences, and the material composition (Figure 4) (Karr 1975; Cotton 1965). At longer wavelengths, near-IR vibrational transitions are affected by composition, the atomic (crystal) structure, and nearest/next neighbor chemistry of the material (Karr 1975; Cotton 1965).

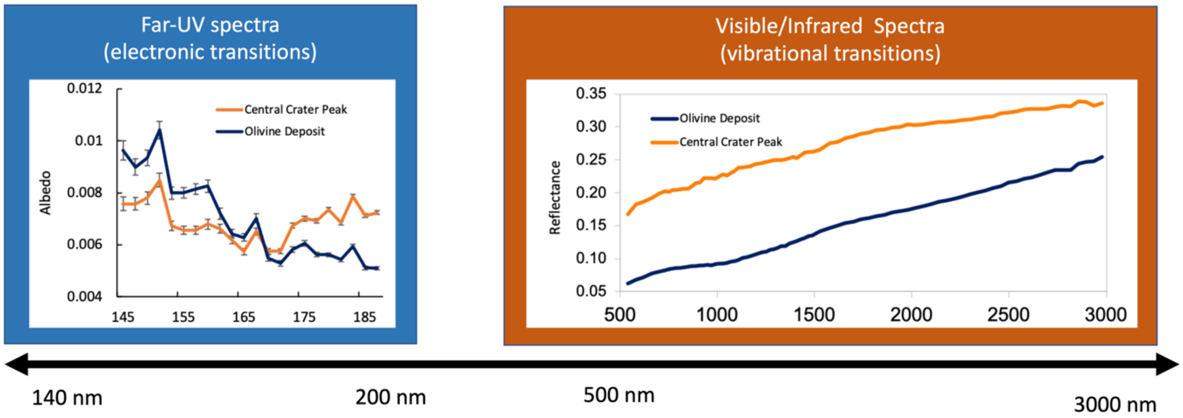

Figure 4: Sample spectra from Aristarchus crater central peak and olivine-bearing rim deposit from (Left) LAMP far-UV spectra and (Right) M^3 near-IR spectra. Far-UV and **visible** electronic transitions are higher energy, and affected by quantum mechanically derived selection rules, species of ion/atoms, and the symmetry of the E-field the atoms experience. Near-IR vibrational transitions are affected by the composition, atomic structure, and nearest neighbor/next neighbor chemistry.

Scattering properties of a material can also have an effect on the far-UV (< 200 nm) spectra of a mineral and are discussed in depth in other LAMP related studies (Byron et al. 2021; Raut et al. 2018; Cahill et al. 2019; Hendrix et al. 2016). Lunar regolith is primarily backscattering at far-UV wavelengths (Raut et al. 2018). "Fluffier" regolith or more porous fairy castle structures can also cause the albedo to be lower across all far-UV wavelengths (Byron et al. 2019; Raut et al. 2018; Gladstone et al. 2012). The results presented and discussed here, as well as previous LAMP studies, demonstrate composition of the lunar regolith has a significant impact on far-UV spectral features (Byron et al. 2021; Byron et al. 2020; Hendrix et al. 2016; Cahill et al. 2019).

Previous far-UV spectra of returned Apollo samples and terrestrial analogs show that plagioclase feldspars has a higher albedo longward of ~170 nm (Figure 5; Wagner et al. 1987; Hapke 1978). Plagioclase feldspar typically has varying amounts aluminum (Al) and alkali metals including potassium (K), sodium (Na) and calcium (Ca) (Table 2). All of these elements can affect the nearest neighbor chemistry of silicate tetrahedra in minerals, and consequently the far-UV spectra. Using transmittance far-UV spectra of amorphous silicate (quartz:SiO_2) and alkali doped glasses, Sigel 1971 found that UV absorption between 150-200 nm is proportional to alkali content and sensitive to the alkali species present. Additionally, this study found aluminum and alkali co-doped glass show a decrease in absorption (or increase in reflection), and suggested that aluminum (Al) atoms can effectively substitute for silicon (Si) in the glass silicate framework. This framework "bridges" two silicate tetrahedrons, with alkali atoms present to maintain charge balance (Sigel 1971).

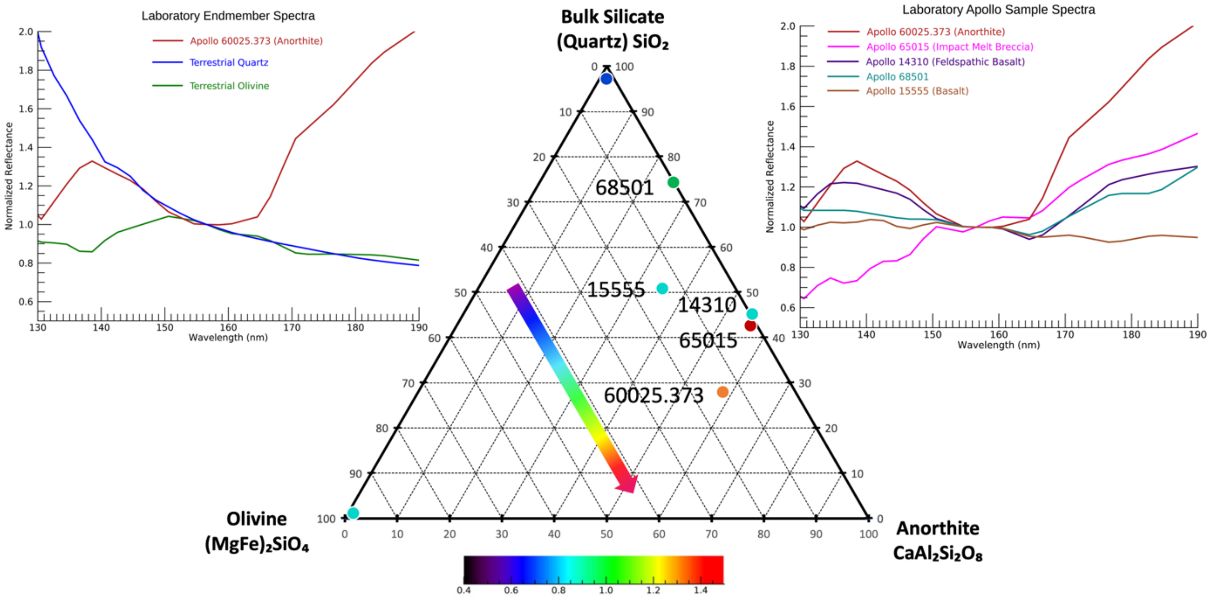

Figure 5: (Center) Compositions (wt.%; Table 2) of Apollo samples on a ternary diagram, with their Off/On band albedo ratios **indicated by color, which corresponding to the axis at the bottom.** (Left/Right) far-UV spectra of various terrestrial endmembers further demonstrating the sensitivity of the far-UV to increased felspathic content. Spectra adapted from Wagner et al.

1987, Hapke et al. 1978, and Philipp 1966. Arrow indicates a general trend of LAMP Off/On band ratio increasing with plagioclase content.

Apollo Sample	Type	Plagioclase (%)	Olivine (%)	SiO_2 (%)	Al (%)	Ca (%)	Na (%)	Off/On Band Ratio
60025.373[a]	Ferroan Anorthosite	70-98	20	44	36.03	19.13	0.034	1.18
65015[b]	Impact melt Breccia	60	0.9	47	19.98	12.03	0.44	1.4
14310[c]	Feldspathic Basalt	60	0	50	20.1	12.03	0.63	0.96
68501[d]	Soil and Rake Residue	13 (2.5 An)	0	45	26.9	15.1	0.36	1.01
15555[e]	Basalt	30	12	44	7.45	9.22	0.24	0.94

Table 2: Apollo Sample compositions and the calculated Off/On band ratio. Spectra for these samples were taken from Wagner et al. 1987. Weight percentages for each sample were taken from the following studies: a)James et al. 1991 and Dixon et al. 1975; b)Simonds et al. 1973 and Hubbard 1973; c)Gancarz et al. 1972 and Hubbard 1973; d)Heiken et al. 1973 and Taylor 1973; e)Longhi et al. 1972 and Chappell 1972.

Electronic transitions associated with alkali-silicate bonds could explain the increase in far-UV albedo longward of 170 nm observed both by the LAMP instrument and previous laboratory studies (Figure 5; Table 2). **As discussed above, Sigel 1971 reported the alkali content of glasses is proportional to the far-UV absorption (Sigel 1971).** Far-UV spectra and composition of Apollo soils show that Off/On band ratios trend upwards with increased plagioclase (aluminum and calcium) content (Figure 5; Table 2). The absorption edge seen in LAMP spectra and Off/On ratios is possibly caused by the presence of the alkali content of feldspathic lithologies (i.e., Na, K, Ca), or at least an alkali-enriched melt (Figure 5; Table 2). The LAMP Off/On band ratio values at Aristarchus central peak (1.15) are higher than other plagioclase-rich areas like Giordano Bruno (0.96) and Tycho crater (0.85), reported by Byron et al. 2020, suggesting it is compositionally different. The abnormally high Off/On band ratios at Aristarchus suggest the plagioclase feldspar identified by both LAMP and M^3 (Figure 3) could be alkalic. The presence of alkalic plagioclase feldspar at Aristarchus is further supported by the Diviner concavity index map (Figure 2), which is consistent with silicate rich material in both the crater central peak, and the Southwest crater rim. Since feldspathic lithologies are typically characterized by the ratio of sodium (Na) and calcium (Ca) present in a given sample, these LAMP spectral features can be used to constrain the relative alkali content in this way for these Aristarchus features and other lunar surface regions of interest.

6. Conclusion

LAMP Off/On band ratios are able to distinguish plagioclase feldspar from minerals such as quartz and mafic minerals. Olivine and pyroxene rich deposits at Aristarchus are dark in the far-UV, and nearly indistinguishable from each other based on LAMP data alone. More work is needed to determine whether far-UV spectra are sensitive to other mafic and/or mafic bearing lithologies. M^3 spectra of the central peak showed the presence of plagioclase and an absence of pyroxene, while LAMP Off/On band ratios are consistent with anorthite in the central peak. Combined observations from LAMP and M^3 spectra show the central peak and high albedo ejecta around Aristarchus contains shocked plagioclase feldspar, possible alkalic, based on LAMP far-UV spectral data which is corroborated by M^3 and Diviner data.

The edge of an absorption band seen in LAMP spectra and Off/On band ratio maps is probably caused by the interaction of the silicate tetrahedra with alkaline atoms. Feldspathic lithologies typically are characterized by the amounts of sodium (Na), potassium (K), or calcium (Ca) present, and the presence of these lithologies explains Byron et al. 2020's previously reported Off/On band values around bright rayed craters. The Off/On band values at Aristarchus crater (1.15) are higher than what was previously reported for other plagioclase-rich craters. This suggests the plagioclase feldspar at Aristarchus is unique, and possibly alkalic. This result supports previous studies which suggested KREEP-rich plagioclase is present at Aristarchus **(Hagerty et al. 2009, Jolliff et al. 2000).** Additional far-UV laboratory studies of alkaline-plagioclase feldspars are needed to support future study of the area and aid in quantifying the alkaline content of the feldspathic material in the ejecta blanket with LAMP.

8. References

Arnold, J.A., Glotch, T.D., Lucey, P.G., et al. 2016, *JGRE*, 121, 1342-1361

Besse, S., Sunshine, J., Staid, M., et al. 2012, *Icar*, 222, 229-242

Braden, S.E., Lawrence, S.J., Robinson, M.S., et al. 2009, *White Paper: Planetary Science Decadal Survey (2013-2022)*

Braden, S.E., Stopar, J.D., Robinson, M.S., et al. 2014, *Nat. Geo.* 7, 787-791

Byron, B.D., Retherford, K.D., Greathouse, T.K., et al. 2019, *JGRE*, 124, 823-836

Byron, B.D. Retherford, K.D., Greathouse, T.K., et al. 2020, *JGRE*, 125, e2019JE006269

Byron, B.D., Retherford, K.D., Czajka, E.A., et al. 2021, *PSJ*, 2:189 (11pp)

Cahill, J. T., Wirth, A. A., Hendrix, A. R., et al. 2019, *JGRE*, 124, 294

Chappell, B.W., Compston, W. et al. 1972, *Sci*, 175, 4020, 415-216

Chevrel, S.D., Pinet, P.C., Daydou, Y., et al. 2009, *Icar*, 199, 9-24

Cotton, F.A., 1965, *Chemical Applications of Group Theory*, Int.Sci. Pub.

Dixon, J.R., Papike, J.J., 1975, *LPSC*, 6, 263-291

Donaldson Hanna,K.L., Cheek, L.C., Pieters, C.M., et al. 2014, *JGR Planets*, 119, 1516-1545

Gaddis, L.R., Staid, M.I., Tyburczy, J.A., et al. 2003, *Icar*, 161, 262-280

Gaddis, L.R., Pieters, C.M., and Hawke, B. R., 1985, *Icar*, 61, 461-489

Gancarz, A.J., Albee, A.L., Chodos, A.A., 1972, *EPSL*, 16, 3, 307-330

Gladstone, G.R., Stern, S.A., Retherford, K.D., et al. 2010, *SSR, 150, 161*

Gladstone, G.R., Retherford, K.D., Egan, A.F., et al. 2012, *JGRE,* 117, E00H04

Glotch, T.D., Jawin, E.R., Greenhagen, B.T., et al. 2021, *PSJ,* 2:136 (15pp)

Glotch, T.D., Lucey, P.G., Bandfield, J.L., et al. 2010, *Sci*, 329(5998), 1510-1513

Green, R.O., Pieters, C., Mouroulis, P., et al. 2011, *JGRE*, 116, E00G19

Greenhagen, B.T., Lucey, P.G., Wyatt, M.B., et al. 2010, *Sci*, 329, 1509-1509

Hagerty, J.J., Lawrence, D.J., Hawke, B.R., Gaddis, L.R., 2009, *JGRE*, 114, E04002

Hapke, B.W., Partlow, W.D., Wagner, J.K., Cohen, A.J. 1978, *LPSC*, V3. (A79-39253 16-91) p. 2935-2947

Hayne, P.O., Hendrix, A.R., Sefton-Nash, E., et al. 2015, *Icar*, 225, 58-69

Heiken, G.H., McKay, D.S., Fruland, R.M., 1973, *LPSC*, 1, 251-265

Hendrix, A.R., Greathouse, T.K., Retherford, K.D., et al. 2016, *Icar*, 273, 68-74

Hendrix, A., Retherford, K.D., Gladstone, G.R., et al. 2012, *JGRE,* 117, E1200

Hubbard, N.J., Rhodes, J.M., Gast, P.W., et al. 1973, *LPSC*, 2, 1297-1312

Hurwitz, D.M., Head, J.W., Hiesinger, H., 2013, *PSS*, 79-80, 1-38

James, O.B., Lindstrom, M.M., McGee, J.J., 1991, *LPSC*, 21, 63-87

Jolliff, B.L., Wiseman, S.A., Lawrence, S.J., et al. 2011, *NG*, 4, 566-571

Karr Jr., C., 1975, *Infrared and Raman Spectroscopy of Lunar and Terrestrial Minerals*, Ac. Pr.

Klima, R.L., Pieters, C.M., Dyar, M.D., 2007, *M&P. Sci,* 42, 235-253

Klima, R.L., Dyar, M.D., Pieters, C.M., 2011, *M&P. Sci,* 46, 379-395

Liu, Y., Retherford, K. D., Greathouse, T. K., et al. 2018, *JGRE*, 123(10), 2550-2563

Longhi, J., Walker, D., Stolper, E.N., et al. 1972, *The Apollo 15 lunar samples*, 131-134

Magaña, L.O., Retherford, K.D., Byron, B.D., et al. 2022, JGR:Planets, 127,11,e2022JE007301

Mustard, J.F., Pieters, C.M., Isaacson, P.J., et al. 2011, *JGRE*, 116, E00G12

McEwen, A.S., Robinson, M.S., Eliason, E.M., et al. 1994, *Sci*, 266, 1858-1862

Neish, C.D., Cannon, K.M., Tornabene, L.L., et al. 2021, *Icar*, 361, 114392

Philipp, H.R. 1966, *SSC*, Vol 4, 73-75

Pieter, C.M., Fischer, E.M., Rode, O., Basu, A. 1993, *JGRE*, 98, 20817-20824

Pieters, C.M., Stankevich, D.G., Shkuratov, Y.G., Taylor, L.A., 2002, *Icar*, 155,285-298

Pieters C.M., Boardman, J. Buratti, B. et al. 2009, *CS*, 96, 4, 500-505

Raut, U., Karnes, P.L., Retherford, K.D., et al. 2018, *JGRE*, 123

Siegel Jr, G. H. 1971, *JPCS*, 32, 2373-2383

Simonds, C.H., Warner, J.L., Phinney, W.C., 1973, *LPSC*, 1, 613-632

Sunshine, J.M. and Pieters, C.M. 1998, *JGRE*, 103, 13675-13688

Taylor, S.R. 1972, *The Moon*, 7, 181-195

Taylor, S.R. 1982, *Planetary Science: A Lunar Perspective,* LPSI

Wagner, J.K. Hapke, B.W., Wells, E.D. 1987, *Icar*, 69, p.14-28

Zhang, F., Zou, Y.L., Zheng, Y.C., Zhu, Y.C., 2014, *Icar*, 227, 132-151

Zisk, S.H., Hodges, C.A., More, H.J., et al. 1977, *The Moon,* 17, 59-99